

CONSTRAINED VIOLENT RELAXATION TO A SPHERICAL HALO

A. MANGALAM,¹ R. NITYANANDA,² AND S. SRIDHAR³

Inter-University Centre for Astronomy and Astrophysics, Postbag 4, Ganeshkhind, Pune 411 007, India

Received 1998 December 9; accepted 1999 June 5

ABSTRACT

Violent relaxation during the collapse of a galaxy halo is known to be incomplete in realistic cases such as cosmological infall or mergers. We adopt a physical picture of strong but short-lived interactions between potential fluctuations and particle orbits, using the broad framework outlined earlier for incorporating incompleteness of the relaxation. We are guided by results from plasma physics, viz., the quasi-linear theory of Landau damping, but allow for significant differences in our case. Crucially, wave particle scattering does not drive the system to an equilibrium distribution function of the exponential type, even in regions of phase space allowed by the constraints. The physical process is mixing without friction in “action” space, for which the simplest possible model is a *constant* phase space density modulated by the constraints. Our distribution function does not use the exponential functions of the energy prevalent in other work, which we regard as inappropriate to collisionless systems. The dynamical constraint of a finite short period of the relaxation process is argued to lead to a $1/T_r$ factor in the distribution function, where T_r is the radial period. The notion of strong potential fluctuations in a core is built in as a cutoff in pericenter (which we find preferable to one angular momentum, the other alternative we explored). The halo of the self-consistent, parameter-free solutions show an r^{-4} behavior in density at large r , an $r^{1/4}$ surface brightness profile in the region $0.1r_e-8r_e$, and a radially anisotropic velocity dispersion profile outside an isotropic core. The energy distribution seen in simulations $N(E)$ singles out the pericenter cutoff model as the most realistic among the variants we have explored. The results are robust to modifications of the period dependence keeping the same asymptotic behavior or to the use of binding energy raised to the power of $3/2$ in place of $1/T_r$.

Subject headings: galaxies: formation — galaxies: halos — galaxies: interactions — galaxies: kinematics and dynamics — galaxies: structure

1. A MODEL OF QUASI-VIOLENT RELAXATION

Elliptical galaxies are expected to have undergone violent relaxation (Lynden-Bell 1967), which is a collisionless process whereby the energies and angular momenta of stars and dark matter particles get redistributed by strong potential fluctuations in such a way that the outcome depends mainly on the macroscopic features of the initial conditions. This concept is supported by N -body experiments where for a range of initial conditions the final state has more or less a universal profile.

One of the insights gained from cold collapse simulations is that a compact region or a core develops, the system partially reexpands, and then in a few crossing times settles into a centrally peaked configuration with most of the mass inside a radius within a fraction of the initial size (van Albada 1982). The potential fluctuations are initially of large amplitude, but they damp out in a few crossing times. Clumpy and cold initial conditions with small values of $2T/W \simeq 0.1$, where T and W are total kinetic and potential energies, are preferred over hot or homogeneous conditions in order to produce final configurations that fit the de Vaucouleurs $\exp - r^{1/4}$ surface density profile better.

The general violent relaxation problem is difficult because the fluctuations have large amplitudes and damp in a few crossing times. Thus there is no small parameter and just a single timescale. The physical process belongs to the broad category of interactions between *waves* (potential

fluctuations) and *particles* (stars or dark matter), wherein the amplitude of the wave is self-consistently determined by the positions of the particles. We start with the limiting case of small amplitudes, and long-lived waves, where we might expect the problem to submit to perturbative methods. However, it is difficult to determine even the linear modes of self-gravitating, collisionless systems; this is because galaxies are spatially inhomogeneous objects. Quasi-neutral plasmas are not subject to this problem, so let us examine the quasi-linear theory of Landau damping of electrostatic waves in collisionless plasmas (cf. § 49 of Lifshitz & Pitaevskii 1981). The focus of the theory is on the slow evolution of the coarse-grained distribution function (DF) of electrons, $f(\mathbf{p}, t)$, where \mathbf{p} is momentum. A key result is that $f(\mathbf{p}, t)$ obeys a diffusion equation in \mathbf{p} -space:

$$\frac{\partial f}{\partial t} = \frac{\partial}{\partial p_\alpha} \left(D_{\alpha\beta} \frac{\partial f}{\partial p_\beta} \right), \quad (1)$$

where the diffusion coefficient, $D_{\alpha\beta}$, is nonzero only in a range of \mathbf{p} corresponding to electrons that are resonant with the perturbations. This diffusion causes smoothing and creates a plateau in $f(\mathbf{p})$. Furthermore, $D_{\alpha\beta}$ is proportional to the energy in the fluctuations; as this energy is absorbed by the resonant electrons, the diffusion itself weakens and $f(\mathbf{p})$ reaches a steady state. The point we wish to make here is that this evidently non-Maxwellian steady state has been reached by a self-regulating diffusive process.

There is of course a basic difference between slow damping of plasma waves and the damping of the oscillations of a violently relaxing galaxy. In the former, the energy in the waves is absorbed by resonant electrons, whereas the very concept of resonance is dubious in the

¹ Present address: Indian Institute of Astrophysics, Bangalore 560034, India; mangalam@iucaa.ernet.in; mangalam@iiap.ernet.in.

² Permanent address: Raman Research Institute, Sadashivanagar, Bangalore 560 080, India; rajaram@rri.ernet.in.

³ sridhar@iucaa.ernet.in.

latter case, because the oscillations are short lived. In a relaxing galaxy, the orbits of particles are expected to be scattered by an oscillating core (Tremaine 1987; Spiegel & Hernquist 1992, hereafter SH). In realistic situations, the deflections are individually large but small in number. Let us, nevertheless, for orientation, initially consider the limit in which each star, or dark matter particle, undergoes many small kicks. Because of this particles move under the combined actions of integrable forces and small kicks that lead to global stochasticity. In stochastic regions of phase space far from islands, the diffusion of actions is well described by a Fokker-Planck (FP) equation. A feature of the FP equation for Hamiltonian kicks is the complete absence of dynamical friction, a result as old as Landau (1937; cf. § 5.4 of Lichtenberg & Lieberman 1983). The FP equation resembles equation (1), where p are the actions. Once again, $D_{\alpha\beta}$ is proportional to the square of the perturbation. The absence of friction implies that a Maxwellian distribution is not the final steady state. In fact, the process being purely diffusive, it is evident that the DF would approach one that is independent of the actions, given a finite volume of phase space and enough time.

We learn from the above examples that in the limit of long-lived, small-amplitude fluctuations, the relaxation of a galaxy is likely to be primarily diffusive in phase space. This relaxation process is very different from collisional relaxation in neutral gases, which is a reflection of the long-range nature of gravitational forces in contrast to the short range of interatomic forces. The distinction is made clearer by using the H -functions introduced by Tremaine, Hénon, & Lynden-Bell (1986). They are actually functionals of the coarse-grained DF, defined as

$$H[f] = -C(f)d^3x d^3v, \quad (2)$$

where $C(f)$ is a convex function. Any mixing process conserving fine-grained phase density, such as collisionless relaxation, will increase $H[f]$. This result needs the assumption that the initial state had the fine- and coarse-grained distribution equal to each other, which applies to the cold collapse simulations with which we are concerned. It does not imply that H increases monotonically (Dejonghe 1987; Sridhar 1987). On the other hand, binary collisional processes, such as those relevant to thermal relaxation in neutral gases, do not conserve phase density and single out a unique H -function, namely, the Boltzmann entropy given by $C(f) = f \ln f$.

We now extrapolate to the case of the large-amplitude, short-lived fluctuations appropriate to violent relaxation. When the “actions” change by large amounts, the mixing process is no longer correctly described by a diffusion equation. However, the relaxation is probably well described by a process of mixing without friction, and an initial DF will spread as far as it can in phase space; the extent and nature of the spreading being determined by dynamical constraints discussed in the following section. We write the DF $= A(\mathcal{E})$ times a factor expressing constraints, where \mathcal{E} is the single-particle binding energy (bound particles have positive \mathcal{E}). In the short duration before freezeout, A spreads out nearly evenly and beyond $\mathcal{E} = 0$ (some particles escape). But in constructing distribution functions of the galaxy we do not include unbound particles. The parallel to diffusion without friction suggests a final state for which $A(\mathcal{E}) = \text{constant}$.

Note that this hypothesis is the simplest choice consistent with the physics of violent relaxation. A similar concept was

proposed by Yankov (1994) to explain turbulent transport in plasmas of tokamaks with a uniform distribution of particles in a region specified by certain constraints of the problem.

2. A PRESCRIPTION FOR $f(\mathcal{E}, J^2)$

The relevant dynamical constraints will clearly depend on the context; for instance, the merger of two galaxies is very likely to be different from the formation of dark halos by cosmological infall over extended periods of time. We now seek the dynamical constraints appropriate to situations such as the cold collapses familiar from numerical simulations (cf. van Albada 1982) which might also carry over to the case of head-on mergers between galaxies. For simplicity, we assume that the relaxed system is spherical and its DF is a function of the energy, \mathcal{E} , and the angular momentum, J . Tremaine (1987) has suggested the following two plausible physical requirements (see also Merritt, Tremaine, & Johnstone 1989, hereafter MTJ; Stiavelli & Bertin 1987):

1. The potential fluctuations last for only a limited time, T_e , which is of order a few crossing times. Hence orbits with radial periods, T_r , exceeding T_e will be underpopulated by a factor $\sim (T_e/T_r)$. In terms of a plausible physical requirement, this is viewed as a uniform filling of those orbital phases which allowed the particle to visit the core in the time T_e and zero elsewhere. Finally, of course, all phases are equally populated in the coarse-grained function, which means a filling proportional to T_e/T_r .

2. The fluctuations are largely confined to a central region or a core of radius r_c . Hence only orbits whose pericenters are smaller than $\sim r_c$ would have visited the region of large potential fluctuations and have had a chance to relax violently. The validity of this will depend strongly on the initial conditions; the collapse of a cold, nearly non-rotating initial configuration is more relevant to this study.

With this motivation, we assume the following form for $f(\mathcal{E}, J^2)$

$$f(\mathcal{E}, J^2) = (\text{function proportional to } 1/T_r \text{ for large } T_r) \\ \times (\text{cutoff in pericenter or } J^2) \times A \quad (3)$$

The first two factors in the distribution function are the dynamical constraints given by requirements 1 and 2, respectively, and the third factor, A , is taken to be a constant as discussed earlier. The first factor $1/T_r$ ensures the continuity of the DF at $\mathcal{E} = 0$, i.e., $f(\mathcal{E}, J^2) = 0$ for $\mathcal{E} \leq 0$. Jaffe (1987) remarked that one asymptotic property of violently relaxed systems is that $N(\mathcal{E})$ should be finite and nonzero at $\mathcal{E} = 0$ because the number of particles ejected from the core should be smooth across $\mathcal{E} = 0$. We show in § 4 that for small \mathcal{E} , the restricted density of states due to the second factor in equation (3) is $\sim \mathcal{E}^{-3/2}$, while $f \sim 1/T_r \sim \mathcal{E}^{3/2}$ (for finite-mass systems), and therefore $N(\mathcal{E}) \sim \mathcal{E}^0$. We define

$$f(\mathcal{E}, J^2) \equiv f_0(\mathcal{E}, J^2)\mathcal{C}A, \quad (4)$$

where f_0 and \mathcal{C} represent the first and second factors in equation (3). In this work, we studied the following closely related models based on equation (3):

1. A model with $f_0(\mathcal{E}) = \mathcal{E}^{3/2}$ was first obtained and used as an input to generate the $1/T_r$ counterpart discussed

below. Details of this model are presented in Appendix A. The dependence of the distribution function on \mathcal{E} and J is explicit, and hence the analytic work can be carried further.

2. $f_0(\mathcal{E}, J^2) = 1/T_r$ is presented in § 5. Here the dependence of the radial period on \mathcal{E} and J has to be derived iteratively from the potential. The models above form a good starting point for successive numerical iterations which we refer to as r_c and J_m models. There is a variant of these models with $f_0(\mathcal{E}, J^2) = 1/(T_r + T_0)$, with an extra parameter T_0 introduced to assess the sensitivity of the results to the functional form of the period cutoff.

All the above models have the asymptotic properties $\rho \sim r^{-4}$, $N(\mathcal{E}) \sim \mathcal{E}^0$ (described above), and surface densities approximating the $r^{1/4}$ law. The form of energy distributions, $N(\mathcal{E})$, at distances larger than the core radius r_c , or the scale radius r_j , are derived for the pericenter model in § 4. In § 5.1 we describe the form of $N(\mathcal{E})$ for the T_r models. This is helpful in picking out the pericenter cutoff models as a better fit to results of simulations. In § 3 we describe the boundaries in the $(\mathcal{E}-J^2)$ -plane required in doing the integrals in the allowed velocity space. The properties of the solutions and comparison to simulations are described in § 6, and we present a discussion in § 7 and conclusions in § 8. The reader interested in first examining the results is urged to go to §§ 6–8 and then return to §§ 3–5 for some details of the construction.

3. PERICENTER AND ANGULAR MOMENTUM CONSTRAINTS IN THE $(\mathcal{E}-J^2)$ -PLANE

For a spherical model, with a distribution function, $f(\mathcal{E}, J^2) = Af_0(\mathcal{E}, J^2)\mathcal{C}$, including a sharp pericenter cutoff at r_c or in angular momentum, J_m , Poisson's equation can be written as

$$\frac{1}{r^2} \frac{d}{dr} \left(r^2 \frac{d\Phi}{dr} \right) = \frac{A}{r^2} \int d\mathcal{E} dJ^2 \left[2(-\mathcal{E} - \Phi) - \frac{J^2}{r^2} \right]^{-1/2} \times f_0(\mathcal{E}, J^2)\mathcal{C}(\eta), \quad (5)$$

where A is a constant that is determined by normalization. The cutoff function, \mathcal{C} , is given by

$$\mathcal{C}(\eta) = \begin{cases} 1, & \eta \leq 1 \\ 0, & \eta > 1, \end{cases} \quad (6)$$

where η equals either r_p/r_c , where $r_p(\mathcal{E}, J^2)$ is the pericenter, and r_c is the cutoff radius or J/J_m , where J_m is the maximum angular momentum. We explore both these constraints here and construct a method to solve the self-consistent models with $f_0(\mathcal{E}, J^2) = 1/T_r$: equation (5), coupled with

$$T_r(\mathcal{E}, J^2) = 2 \int_{r_p}^{r_a} dr [2(-\mathcal{E} - \Phi) - J^2/r^2]^{-1/2}, \quad (7)$$

where r_p and r_a are the turning points. We have solved the coupled equations by a semianalytical method whose details are presented in § 5.

Now we introduce a variable, $r_0(J^2)$, which is the radius of a circular orbit for a given angular momentum, $J^2 = r_0^3 \Phi_0$. This is useful in determining the region of integration in the $(\mathcal{E}-J^2)$ -plane. Note that $J^2 = M(r_0)r_0$ from Poisson's equation, where $M(r)$ is the mass inside r , and hence it is a monotonically increasing function of r_0 . Figure 1 shows a

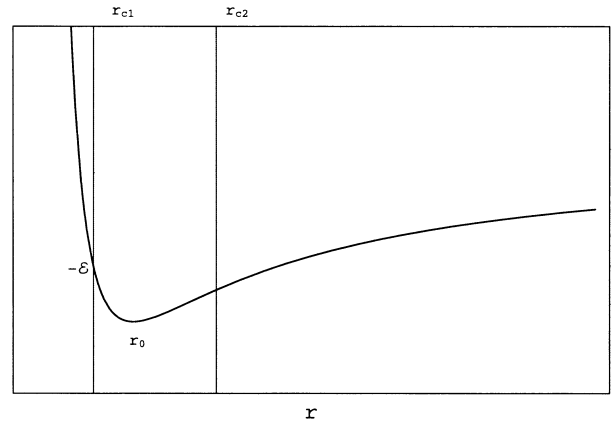


FIG. 1.—Two possible locations of r_c , $r_{c1} < r_0$, and $r_{c2} > r_0$ are indicated in the figure where r_0 is the circular orbit radius. The allowed orbits are those for which $\mathcal{E} \leq \mathcal{E}_f(r_c, r_0)$, as indicated in the figure, and $\mathcal{E} \leq \mathcal{E}_f(r_0, r_0)$, the energy of the circular orbit, respectively.

plot of the absolute value of the effective potential, $-\mathcal{E}_f(r, r_0) \equiv \Phi + J^2/(2r^2) = \Phi + \Phi_0 r_0^3/(2r^2)$, for a given J^2 and a typical Φ . We now consider the region of integration allowed by $\mathcal{C}(\eta)$.

3.1. The Case of $\eta = r_p/r_c$

The region of integration in the $(\mathcal{E}-J^2)$ -plane is bounded by following curves which are shown in Figure 2:

1. The upper bound of the region of interest is given by the minimum of the effective potential ($-\mathcal{E}_f$) of a circular orbit for a given $\Phi(r)$ and r_0 , i.e., $\mathcal{E} < \mathcal{E}_f(r_0, r_0) = -\Phi_0 - \Phi_0 r_0/2$ for $r_p \leq r_0 \leq r_c$. The orbits with $r_p \leq r_c \leq r_0$ obey the bound $\mathcal{E} < \mathcal{E}_f(r_c, r_0) = -\Phi_c - \Phi_0 r_0^3/(2r_c^2)$ as indicated in Figure 1.

2. At a given radius r for the system, the effective potential is bounded by $\mathcal{E} \leq B(r, J^2) \equiv \mathcal{E}_f(r, r_0) = -\Phi - J^2/(2r^2)$ or, equivalently, $v_r^2(r) \geq 0$.

For $r < r_c$, the pericenter constraint is satisfied and the operative bound is just $\mathcal{E} < \mathcal{E}_f(r, r_0)$. Hence, the bounding line $\mathcal{E} = \mathcal{E}_f(r_c, r_0)$ given by constraint 2 lies inside and is tangent to the curve given by constraint 1; the point of contact represents a circular orbit for a given r_0 .

Now consider the case $r > r_c$. The point of intersection (\mathcal{E}_*, J_*^2) between the bounding line of bound constraint 2,

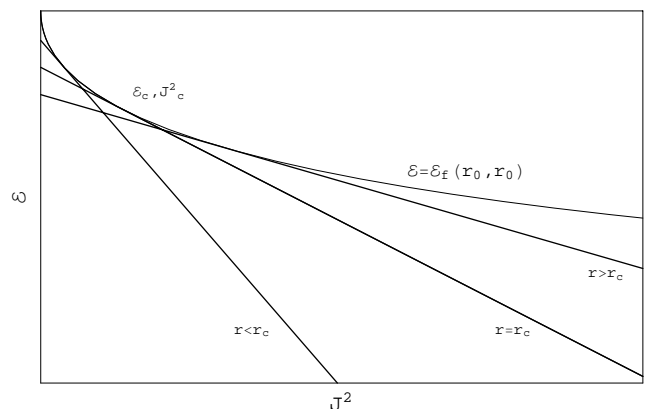


FIG. 2.—Applicable bound for $r < r_c$ is the circular orbit energy, $\mathcal{E}_f(r_0, r_0)$, and for $r > r_c$, it is given by $\mathcal{E} < \mathcal{E}_f(r_c, r_0)$ as explained in Fig. 1. Lines of turning points are drawn for $r > r_c$, $r < r_c$, and $r = r_c$.

$\mathcal{E} = \mathcal{E}_f(r, r_0)$, and $\mathcal{E} = \mathcal{E}_f(r_c, r_0)$, given by bound constraint 1, represents an orbit whose turning points are r and r_c (see Fig. 2). The point of intersection works out to be

$$\mathcal{E}_* = (\Phi_c r_c^2 - \Phi r^2)/(r^2 - r_c^2), \quad (8)$$

$$J_*^2 = 2(\Phi - \Phi_c)r^2 r_c^2/(r^2 - r_c^2). \quad (9)$$

Effectively, for $r > r_c$, the bound given by constraint 2, $\mathcal{E} < \mathcal{E}_f(r, r_0)$, applies up to $J_c^2 = r_c^3 \Phi'_c$, beyond which the bound, $\mathcal{E} < -\Phi_c - J^2/(2r_c^2)$, given by constraint 1, is operative and forms a wedge-shaped region. For $r < r_c$, the region of integration is given by the bound $\mathcal{E} < \mathcal{E}_f(r, r_0)$ and is a triangular-shaped region. The regions of integration are shown in Figure 3 and are summarized by

$$\mathcal{A}_1 \equiv \mathcal{E} < -\Phi - J^2/(2r^2), \quad r \leq r_c, \quad (10)$$

$$\mathcal{A}_2 \equiv \begin{cases} \mathcal{E} < -\Phi - J^2/(2r^2), & r > r_c \text{ and } J^2 < J_*^2 \\ \mathcal{E} < -\Phi_c - J^2/(2r_c^2), & r > r_c \text{ and } J^2 > J_*^2 \end{cases}. \quad (11)$$

Now that the regions of integration have been determined, we can write the integral on the right-hand side of equation (5), without the normalization constant A , as

$$\mathcal{I}(r; f_0) = \begin{cases} \mathcal{I}_0(r; f_0), & r \leq r_c \\ \mathcal{I}_0(r; f_0) - \mathcal{I}_-(r; f_0) + \mathcal{I}_+(r; f_0), & r > r_c \end{cases}, \quad (12)$$

where $J_e^2(r) = -2\Phi r^2$ is the intercept on the J^2 -axis and

$$\mathcal{I}_0(r; f_0) = \frac{1}{r^2} \int_0^{J_e^2} dJ^2 \int_0^{B(r, J^2)} d\mathcal{E} \times \left[2(-\mathcal{E} - \Phi) - \frac{J^2}{r^2} \right]^{-1/2} f_0(\mathcal{E}, J^2), \quad (13)$$

$$\mathcal{I}_-(r; f_0) = \frac{1}{r^2} \int_{J_*^2}^{J_e^2} dJ^2 \int_0^{B(r, J^2)} d\mathcal{E} \times \left[2(-\mathcal{E} - \Phi) - \frac{J^2}{r^2} \right]^{-1/2} f_0(\mathcal{E}, J^2), \quad (14)$$

$$\mathcal{I}_+(r; f_0) = \frac{1}{r^2} \int_0^{\mathcal{E}_*} d\mathcal{E} \int_{J_*^2}^{-(\mathcal{E} + \Phi_c)2r_c^2} dJ^2 \times \left[2(-\mathcal{E} - \Phi) - \frac{J^2}{r^2} \right]^{-1/2} f_0(\mathcal{E}, J^2). \quad (15)$$

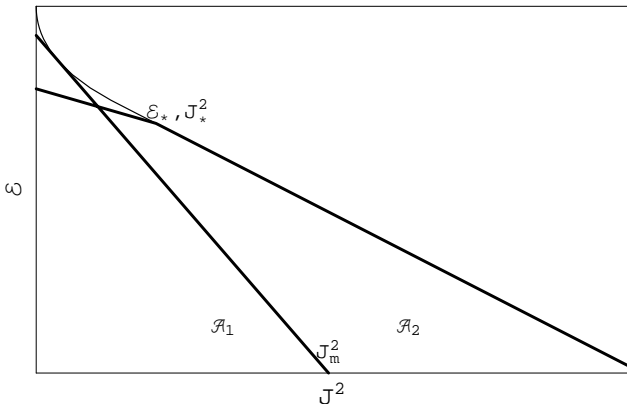


FIG. 3.—Areas of integration enclosed by the bold lines. The triangle-shaped \mathcal{A}_1 , for $r < r_c$, and the wedge-shaped \mathcal{A}_2 , for $r > r_c$, are indicated in the figure. The limits used in evaluating the \mathcal{I} integrals, \mathcal{E}_* , J_*^2 , and J_m are also indicated. The \mathcal{E} intercept is $-\Phi(r)$, and the foot of \mathcal{A}_2 is $-2\Phi_c r_c^2$.

3.2. The Case of $\eta = J/J_m$

Constraint 2 applies here, and the maximum allowed angular momentum is J_m . There are no circular orbits allowed outside the radius t given by $J_m^2 \equiv -2\Phi_j r_j^2 = t^3 \Phi'(t)$. Also, for $r < r_j$ only constraint 2 applies, and for $r > r_j$, the orbits with $J^2 > J_m^2$ are excluded. Hence the region of integration, \mathcal{B} is given by

$$\mathcal{B}_1 \equiv \mathcal{E} < -\Phi - J^2/(2r^2) \quad r < r_j, \quad (16)$$

$$\mathcal{B}_2 \equiv \mathcal{E} < -\Phi - J^2/(2r^2) \text{ and } J^2 < J_m^2 \quad r > r_j.$$

For $\eta = J/J_m$, the integral on the right-hand side of equation (5), without the normalization constant A , will reduce to

$$\mathcal{K}(r; f_0) = \begin{cases} \mathcal{I}_0(r; f_0), & r \leq r_j \\ \mathcal{I}_0(r; f_0) - \mathcal{K}_-(r; f_0), & r > r_j \end{cases}, \quad (17)$$

where

$$\mathcal{K}_-(r; f_0) = \frac{1}{r^2} \int_{J_m^2}^{J_e^2} dJ^2 \int_0^{B(r, J^2)} d\mathcal{E} \times \left[2(-\mathcal{E} - \Phi) - \frac{J^2}{r^2} \right]^{-1/2} f_0(\mathcal{E}, J^2). \quad (18)$$

4. RESTRICTED DENSITY OF STATES FOR A PERICENTER CUTOFF

Here we calculate the density of states for a model that has a sharp pericenter cutoff. The restricted density of states is given by

$$g(\mathcal{E}) = \int d^3r \mathcal{C} \frac{r_p}{r_c} \frac{d^3v}{d\mathcal{E}}$$

$$= 8\pi^2 \int_{\mathcal{A}} dr \int_0^{J_{\max}^2} dJ^2 / \sqrt{2(-\mathcal{E} - \Phi) - J^2/r^2}$$

$$= 16\pi^2 \sqrt{2} \int_{\mathcal{A}} r dr$$

$$\times \left[\sqrt{(-\mathcal{E} - \Phi)r^2} - \sqrt{(-\mathcal{E} - \Phi)r^2 - \frac{J_{\max}^2}{2}} \right], \quad (19)$$

where J_{\max}^2 is determined by constraints. Hereafter we work with units where $GM = 1$. There is no contribution to $g(\mathcal{E})$ from $\mathcal{E} > -\Phi$ and therefore for a given energy \mathcal{E} , only the region $r < r_e$ is accessible where $\Phi(r_e) = -\mathcal{E}$. Consult Figure 3 for the allowed range of integration, \mathcal{A} . For $r < r_c$, the pericenter constraint 1 is satisfied and therefore $J_{\max}^2 = J_e^2 = 2(-\mathcal{E} - \Phi)r^2$, as given by constraint 2. Now take the case when $\mathcal{E} > \mathcal{E}_c$ and $r > r_c$, shown in Figure 4, where $\mathcal{E}_c \equiv -\Phi_c - \Phi'_c r_c/2$, the energy of the circular orbit of radius r_c . Earlier, the point of intersection of $-\Phi - J^2/(2r^2)$ and $-\Phi_c - J^2/(2r_c^2)$ was defined to be \mathcal{E}_* , J_*^2 . Here $\mathcal{E} > \mathcal{E}_c > \mathcal{E}_*$, and hence the pericenters lie inside r_c and $J_{\max}^2 = J_e$ as given by constraint 2. Now consider the case $\mathcal{E} < \mathcal{E}_c$ and $r > r_c$ as illustrated in Figure 5 for which $J_c^2 = -2(\mathcal{E} - \Phi_c)r_c^2 < J_*^2$. It is clear that $J_{\max}^2 = \min(J_c^2, J_e^2)$, and if $J_c^2 < J_e^2$, the particle has a $J_{\max}^2 = J_c^2$ because any higher angular momentum will include orbits whose pericenters lie outside r_c . This happens only for $r_c < r < r_I$, where $r_I(\mathcal{E}, r_c)$

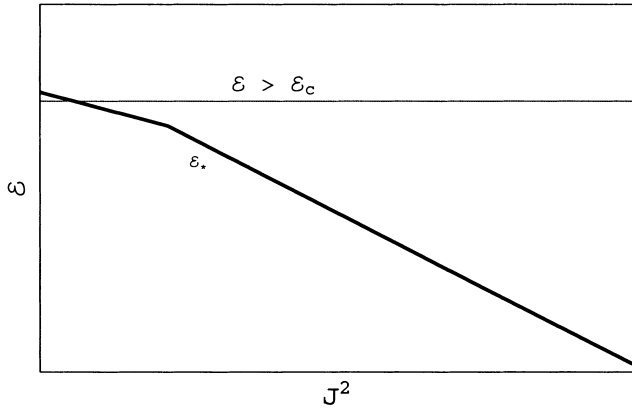


FIG. 4.— $J_{\max}^2(\mathcal{E}, r)$ for the case $\mathcal{E} > \mathcal{E}_c$ and $r > r_c$ is at the point of intersection. In this case, $\mathcal{E} > \mathcal{E}_*$, since $\mathcal{E}_c > \mathcal{E}_*$. This implies that $J_{\max}^2 = J_c^2 = -2(\mathcal{E} + \Phi)r^2$. When $r < r_c$, the pericenter constraint is satisfied and hence $J_{\max}^2 = J_c^2$.

is the apocenter of an orbit for a given energy $-\mathcal{E}$ and pericenter r_c . It is given by

$$\mathcal{E} = \frac{\Phi_I r_I^2 - \Phi_c r_c^2}{r_I^2 - r_c^2}, \quad (20)$$

which has two roots; we seek the one for which $r_I > r_c$. To summarize

$$J_{\max}^2(\mathcal{E}, r) = \min(J_c^2, J_\epsilon^2) = 2 \begin{cases} (-\mathcal{E} - \Phi)r^2, & -\Phi > \mathcal{E} > \mathcal{E}_c, r < r_\epsilon, \\ (-\mathcal{E} - \Phi_c)r_c^2, & \mathcal{E}_c > \mathcal{E}_* > \mathcal{E}, r_c < r < r_I < r_\epsilon, \\ (-\mathcal{E} - \Phi)r^2, & \mathcal{E}_c > \mathcal{E} > \mathcal{E}_*, r_c < r_I < r < r_\epsilon. \end{cases} \quad (21)$$

We may then write

$$g(\mathcal{E}) = 16\pi^2 \sqrt{2} \left[-g_c(\mathcal{E}) + \int_0^{r_\epsilon} r^2 \sqrt{-\mathcal{E} - \Phi} dr \right], \quad (22)$$

where

$$g_c(\mathcal{E}) = \begin{cases} \int_{r_c}^{r_I} dr r^2 \sqrt{\mathcal{E}_* - \mathcal{E}(1 - r_c^2/r^2)^{1/2}} \\ \mathcal{E}_c > \mathcal{E}_* > \mathcal{E} \quad r_c < r < r_I < r_\epsilon \\ 0 \quad \text{otherwise} \end{cases} \quad (23)$$

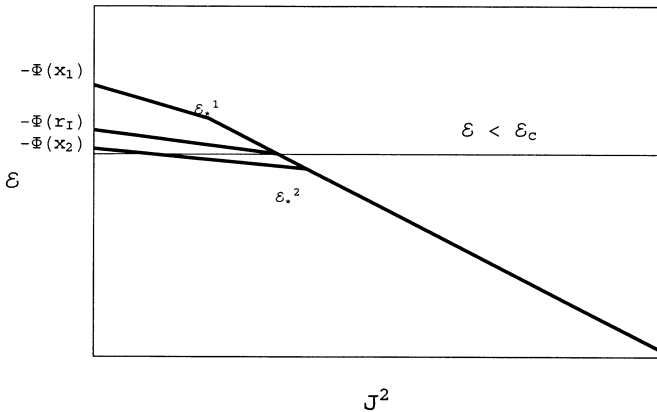


FIG. 5.— $J_{\max}^2(\mathcal{E} > \mathcal{E}_c, r)$ for $\mathcal{E}_* > \mathcal{E}$ and $\mathcal{E}_* < \mathcal{E}$ are shown in the figure. $\mathcal{E}_c > \mathcal{E}_2 > \mathcal{E}_*$ for a radius $r = x_2 > r_c$ and $J_{\max}^2 = -2(\mathcal{E} + \Phi)r^2$, given by the point of intersection at the energy $\mathcal{E} > \mathcal{E}_c$. Similarly, $\mathcal{E} < \mathcal{E}_* < \mathcal{E}_c$ for $r = x_1 > r_c$ and $J_{\max}^2 = -2(\mathcal{E} + \Phi_c)r_c^2$. Also $r_c < x_1 < r_I < x_2$, where r_I , given by $(\mathcal{E} - \Phi_I)r_I^2 = (\mathcal{E} - \Phi_c)r_c^2$, is the apocenter of an orbit with energy $-\mathcal{E}$ and pericenter r_c .

We can now use the equation above to calculate the density of states and the energy distribution for a Keplerian potential, the asymptotics of which are applicable more generally for finite-mass systems. After some algebra, the restricted Keplerian density of states (in units where $GM = 1$) is given by

$$g_k(\mathcal{E}) = \pi^3 \sqrt{2} \begin{cases} \mathcal{E}^{-5/2}, & \mathcal{E} \geq \mathcal{E}_c \\ -4\mathcal{E}^{-3/2} \Phi_c r_c^2 (1 - \mathcal{E} \Phi_c r_c^2), & \mathcal{E} < \mathcal{E}_c, \end{cases} \quad (24)$$

where it is continuous at $\mathcal{E}_c = 1/(2r_c)$. The energy distribution for $f_0(\mathcal{E}) = A'\mathcal{E}^{3/2}$ will then go as

$$N_k(\mathcal{E}) = A'\pi^3 \sqrt{2} \begin{cases} \mathcal{E}^{-1}, & \mathcal{E} \geq \mathcal{E}_c \\ 4\Phi_c r_c^2 (1 - \mathcal{E} \Phi_c r_c^2), & \mathcal{E} < \mathcal{E}_c. \end{cases} \quad (25)$$

Note that for any finite-mass potential, the above equations are valid for a large radius ($r \gg r_c$) and only approximate in the inner region where the realistic potential deviates from $1/r$. Clearly, as $r_c \rightarrow \infty$, $\mathcal{E}_c \rightarrow 0$, and one recovers the Keplerian form of $g(\mathcal{E}) \propto \mathcal{E}^{-5/2}$, and if r_c is zero then $g(\mathcal{E})$ vanishes as expected. Near small \mathcal{E} , the velocities become more radial and the unconstrained Keplerian density of states, $\mathcal{E}^{-5/2}$, is reduced by a factor $v_r^2 \propto \mathcal{E}$. In our model the assumption of a sharp pericenter cutoff at r_c leads to $g(\mathcal{E}) \propto \mathcal{E}^{-3/2}$ near $\mathcal{E} = 0$ and the choice of $f(\mathcal{E}) = 1/T_r \sim \mathcal{E}^{3/2}$, at small \mathcal{E} , based on the dynamical arguments made earlier, is consistent with the required property of the “break of $N(\mathcal{E} = 0)$,” or the finite and nonzero value of $N(\mathcal{E} = 0)$. Jaffe (1987) made the interesting point that the demand of a break in $N(\mathcal{E}) = f(\mathcal{E})g(\mathcal{E})$ at $\mathcal{E} = 0$ for an (unrestricted) Keplerian density of states, leads to $f(\mathcal{E}) \sim \mathcal{E}^{5/2}$ near $\mathcal{E} = 0$, and as a result, the density behaves as $\Phi^4 \propto r^{-4}$. The self-consistent r_c models and the J_m models (§ 5) presented here are infinite-radius and finite-mass models with an r^{-4} density profile. We have checked that the finite and nonzero $N(\mathcal{E} = 0)$ property also holds for the angular momentum restricted density of states.

5. THE $f_0 = 1/T_r$ MODEL

The numerical solution of Poisson’s equation for $f_0 = 1/T_r$ follows closely the analytics in § 3. The areas of integration in (\mathcal{E}, J^2) space are determined by equations (12) and (18). Starting with the initial guess of the potential given in Appendix A or the corresponding one for angular momentum cutoff, the radial period $T_r(\mathcal{E}, r_0)$ is calculated by a root solving and integration routine within the bound given by $\mathcal{E} < \mathcal{E}_f(r_0, r_0)$ for $r_0 < r_c$ and $\mathcal{E} < \mathcal{E}_f(r_c, r_0)$ for $r_0 > r_c$ in case of the r_c model. Similarly, the bound $\mathcal{E} < \mathcal{E}_f(r_0, r_0)$; $r_0 < r_{\max}(\mathcal{E})$ was used in the case of the J_m model where $r_{\max}(\mathcal{E})$ is the radius of the largest allowed circular orbit. A lookup (interpolation) table for $T_r(\mathcal{E}, r_0)$ was prepared. For a given radius, r , the regions of integration are determined by \mathcal{A} or \mathcal{B} , and then the distribution function $1/T_r$ is integrated to calculate the density profile using

$$\frac{1}{r^2} \frac{d}{dr} \left(r^2 \frac{d\Phi}{dr} \right) = K \begin{cases} \mathcal{A}(r; T_r^{-1}) & r_c \text{ model} \\ \mathcal{B}(r; T_r^{-1}) & J_m \text{ model} \end{cases}, \quad (26)$$

$$T_r(\mathcal{E}, J^2) = 2 \int_{r_p}^{r_a} dr [2(-\mathcal{E} - \Phi) - J^2/r^2]^{-1/2}, \quad (27)$$

where r_p and r_a are the turning points and the value of K is chosen so that the total mass is 1 and $G = 1$. The next iterate of the potential is then trivially obtained from

$$\Phi(\xi) = - \int_{\xi}^{\infty} \xi^{-2} \mathcal{M}(\xi) d\xi, \quad (28)$$

where $\mathcal{M}(\xi)$ is the mass fraction inside ξ that is calculated from the density, the right-hand side of equation (26). Here, $\Phi(\infty)$ is taken to be zero to be consistent with the initial guess of $\mathcal{E}^{-3/2}$ for the radial period.

The numerical code was used to verify the $\mathcal{E}^{3/2}$ solution (the initial guess) and vice versa. A high-precision routine was used to calculate the radial period for an arbitrary potential, and this was tested against the well-known forms for isochrone and Kepler potentials and found to be precise to within a millionth of the correct value. The verification of the analytics established the robustness of the numerics used. The numerical scheme converges rapidly to a solution in a few iterations. This indicates that the properties of these models are close to those of the $\mathcal{E}^{3/2}$ models. Figure 6 illustrates that the r_c model is nearly isochronic. For many purposes, one could have been satisfied with the $\mathcal{E}^{3/2}$ models, which are much easier to implement than the $1/T_r$ models, for exploratory work. But this is strictly with the hindsight provided by our constructing the models in the first place.

5.1. The Energy Distribution

Let us now look at the energy distribution, $N(\mathcal{E})$. For a spherical system with the distribution, $f(\mathcal{E}, J^2)$, one can write the differential energy distribution (see Binney & Tremaine, eq. [4P-11]) as

$$N(\mathcal{E}) = 4\pi^2 \int f(\mathcal{E}, J^2) T_r(\mathcal{E}, J^2) dJ^2. \quad (29)$$

In the case of $f = A \mathcal{G}(\eta)/T_r$, we obtain

$$N(\mathcal{E}) = 4\pi^2 A \int \mathcal{G}(\eta) dJ^2 = 4\pi^2 A J_{\eta}^2(\mathcal{E}), \quad (30)$$

where $J_{\eta}^2(\mathcal{E})$ is the constraint boundary in the $(\mathcal{E}-J^2)$ -plane. In the case of the r_c model, the shape of the constraint in this plane (cf. constraint 1, § 3.1) determines the energy distribution which is given by

$$N_c(\mathcal{E}) = 4\pi^2 A \begin{cases} t^3 \Phi'(t), & \text{where } -\Phi(t) - t\Phi'(t)/2 = \mathcal{E}, \\ & \mathcal{E} > \mathcal{E}_c \\ -2(\mathcal{E} + \Phi_c)r_c^2, & \mathcal{E} < \mathcal{E}_c, \end{cases} \quad (31)$$

where \mathcal{E}_c is the energy of a circular orbit at r_c as defined in § 4, and similarly for J_m model (cf. § 3.2), we obtain

$$N_f(\mathcal{E}) = 4\pi^2 A \begin{cases} t^3 \Phi'(t), & \text{where } -\Phi(t) - t\Phi'(t)/2 = \mathcal{E}, \\ & \mathcal{E} > \mathcal{E}_m \\ J_m^2, & \mathcal{E} < \mathcal{E}_m, \end{cases} \quad (32)$$

where the energy \mathcal{E}_m of the largest allowed circular orbit is given by

$$\mathcal{E}_m = -\Phi(t) - t^2 \Phi'(t)/2, \quad t^3 \Phi'(t) = J_m^2. \quad (33)$$

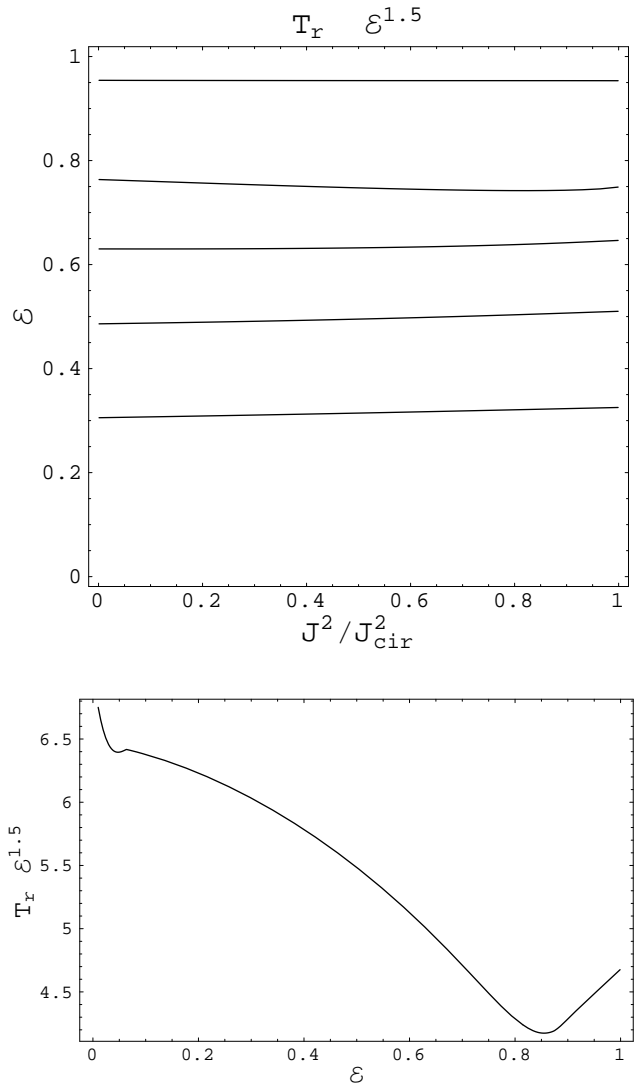


FIG. 6.—*Top*: Contour plot of the variation of $T_r \mathcal{E}^{3/2}$ in the allowed $(\mathcal{E}-J^2)$ -plane. The flat contours indicate that T_r is very nearly isochronic and close to $\mathcal{E}^{-3/2}$. *Bottom*: The deviation is depicted which shows a section taken at $J^2/J_{\text{cir}}^2 = 0.5$, where $J_{\text{cir}}^2(\mathcal{E})$ is the angular momentum of a circular orbit at a given energy, \mathcal{E} .

The Keplerian limit of equations (31) and (32) agrees exactly with the Keplerian limits of $\mathcal{E}^{3/2}$ counterparts, when one takes into account the fact that for a Kepler potential, $T_r = \pi GM \mathcal{E}^{-3/2} / \sqrt{2}$. Therefore $A/A' = \pi/\sqrt{2}$ in units where $GM = 1$. It is clear that, near small \mathcal{E} , the form of $N(\mathcal{E})$ is linear for the r_c model and the slope is $-8\pi^2 A r_c^2$ [positive in $N(\mathcal{E})$] while the $N(\mathcal{E})$ is flat for the J_m model. From the dynamical arguments in § 2 we expect orbits with small T_r to be more populated than the ones with larger radial periods. However, we have no reason to adhere to the strict $1/T_r$ form for small T_r . It is worth checking how sensitive our results are to a modification in which f_0 is flatter at small T_r while retaining the $1/T_r$ asymptotic behavior. We thus try

$$f_0(E, J^2) = \frac{1}{T_r + T_0}, \quad (34)$$

where T_0 is a parameter which is chosen to be of the order of the radial period of the harmonic oscillator, T_h , near the

bottom of the well and given by

$$T_h = \frac{\pi}{\sqrt{\Phi''(0)}}. \quad (35)$$

Again, the maximum deviation from the initial guess up to the second iterate in the density was found to be less than 1% for $T_0 = 0.5T_h, 1T_h, 2T_h$. This indicates that the distribution function is probably stable and insensitive to small changes in f_0 but sensitive to the choice of the constraint, $\mathcal{C}(\eta)$. This and the similarity of the $\mathcal{E}^{3/2}$ models to the $1/T_r$ counterparts can be explained by the fact that f_0 is dominated by $\mathcal{E}^{3/2}$ (see the contour plot of $T_r \mathcal{E}^{3/2}$, Fig. 6).

6. PROPERTIES OF THE SOLUTIONS AND COMPARISON WITH SIMULATIONS

We discuss the analytic results in the preceding sections and the properties of the r_c and J_m solutions and compare it with relevant simulations and the $r^{-1/4}$ law. As mentioned in § 1, the simulations of direct relevance are cold collapse simulations, in particular the C runs of van Albada (1982), who has presented the density, $N(\mathcal{E})$, velocity dispersion, and anisotropy profiles of the final configurations. In our Figures 1, 2, 3, 4, and 5 a Henon isochrone potential was used to illustrate the allowed region in phase space.

Scaled quantities and their physical units.—The models have two free parameters, the total mass M and either the cutoff radius r_c or a maximum value of angular momentum J_m . Below, we compare the r_c models with the J_m models. The scale radius, r_s , is the scale radius of the J_m model and equals the core radius, r_c , in the r_c model. If the total mass and scale radius are set to unity, the model has no free parameters.

The potential in the r_c solution is scaled according to

$$\Phi = \frac{GM}{ar_c} \theta = 0.265 \frac{GM}{r_c} \theta, \quad (36)$$

and similarly the scale for potential in the J_m model is $0.462GM/r_s$. The density scales as $(1/4\pi a)M/r_c^3 = 0.021M/r_c^3$ for the r_c model whereas it scales as $0.0368M/r_s^3$ for the J_m model. The radial orbit period can be written as

$$T_r = \frac{2r_c}{\sqrt{\alpha}} \int_{\xi_1}^{\xi_2} \frac{d\xi}{\sqrt{-\mathcal{E} - \Phi(\xi) - J^2/2\xi^2}}, \quad (37)$$

and hence we define a unit, $T_c \equiv 2r_c/\sqrt{\alpha} = 2\sqrt{a}\sqrt{r_c^3/GM}$. For the r_c model, $a = 3.38$ ($T_c = 3.68$) and $a = 2.16$ ($T_c = 2.94$).

The density profile.—For large r , the densities, $\rho(r)$, for both the models scale as r^{-4} ; this has been derived analytically in Appendix A and is also apparent from Figure 7. The density has a sharp break at $r = r_c$ for the r_c models. The fraction of mass in the core is about 5% for both models. The density continues to decrease gently with r up to about $5r_c$, beyond which the slope changes rather abruptly to a much steeper value and rapidly converges to the asymptotic r^{-4} profile (see the log-log plot in the lower panel of Fig. 7). The radius at which the break occurs is a few r_s (see eq. [A14]) for both models. This is seen in the C runs of van Albada (1982, see Fig. 6 in the paper). A similar break is also seen in the cosmological simulations of Tormen, Bouchet, & White (1997) and Moore et al. (1998) where the

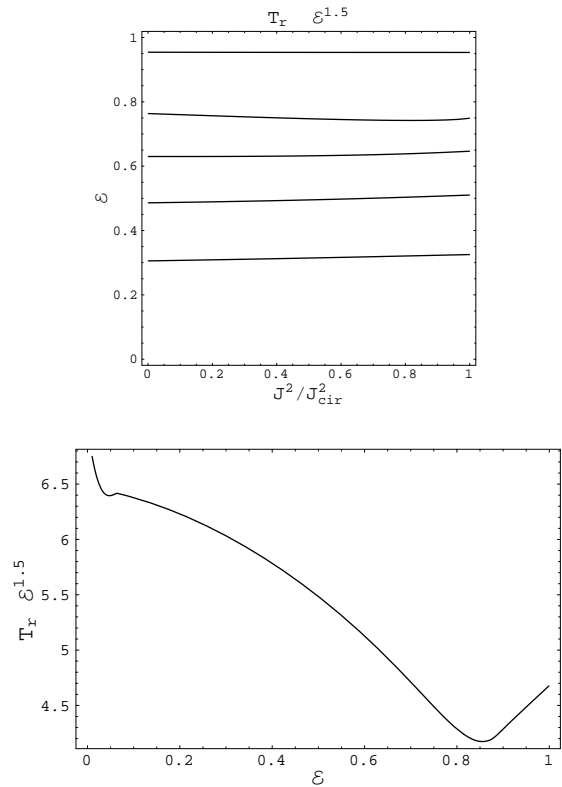


FIG. 7.—Top: Density as a function r/r_s , where $r_s = r_c$ for the r_c models and r_s is the scale radius of the J_m models. The former shows a sharp drop at r_c due to the pericenter constraint, whereas the latter has a smooth profile. Bottom: The log-log plot shows a break near $5r_c$ and an asymptotic form of r^{-4} from $10r_c$ to $100r_c$ for both models. The density is shown in units of $0.021M/r_c^3$ for the r_c model and $0.0368M/r_s^3$ for the J_m model.

power law is roughly r^{-1} for the inner region and between r^{-3} and r^{-4} for the halo.

The differential energy distribution.—Here we use $E = -\mathcal{E}$ in order to compare our results with simulations. The differential energy distribution, $N(E)$, is a useful indicator of the phase space structure. The differences in the analytic forms of $N(E)$ for the different constraints are indicated by equations (25), (31), and (32) which corroborate each other in the Keplerian limit [this is a reflection of the shape of the $\mathcal{C}(\eta)$ in the $(\mathcal{E}-J^2)$ -plane]. Whereas the real space structure (especially at large r) for the two models is similar, the plots in Figure 8 demonstrate how different the models are at high energies; $N(E)$ for the J_m model rises sharply, reaches a maximum at some E , and thereafter is independent of E . For the r_c model, $N(E)$ is smooth, rising gradually, and becomes a strictly linear function of E (see Fig. 7 of van Albada 1982, runs C2 and C3 for a linear plot). The linear region in our model begins at energies 0.7 of the well depth (cf. Appendix A), i.e., it is dominantly linear and is consistent with C2 and C3. The log plot of Figure 8 is also consistent with Figure 4-20 in Binney & Tremaine of run C3 and the simulations of Spiegel & Hernquist (1992, their Fig. 2). Also it is clear from equation (30) that the nonzero intercept of the constraint, $\mathcal{C}(\eta)$, which is $J_m^2(\mathcal{E} = 0)$, has the desirable effect of implementing Jaffe's (1987) insight that the differential energy distribution $N(E)$ tends to a nonzero value as $E \rightarrow 0$ from below, since the probability of ejection from the core is not expected to be sensitive to small changes in the final energy.

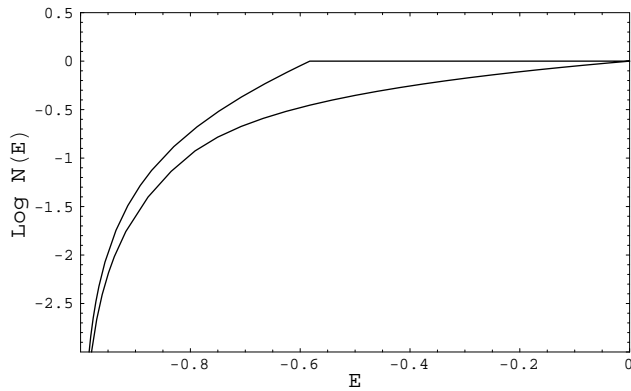


FIG. 8.— $N(E)$ for the J_m model rises abruptly and then is flat, whereas the $N(E)$ for the r_c model increases gradually. The well depth in both cases was taken to be 1.

De Vaucouleurs' $r^{1/4}$ law.—In both cases, the surface densities provide reasonably good fits to the de Vaucouleurs' $r^{1/4}$ law in the range $0.1r_e - 8r_e$ as indicated in Figure 9, assuming a constant mass-to-light ratio. This includes the range in

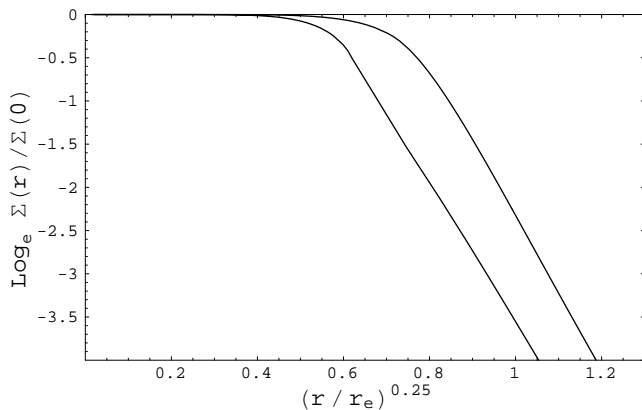


FIG. 9.—Surface density, Σ , is an excellent fit to the $r^{1/4}$ law for $0.1 < r/r_e < 8$; $r_e = 6.65r_s$ for the r_c models (lower curve), and $r_e = 4.03r_s$ for the J_m models (upper curve).

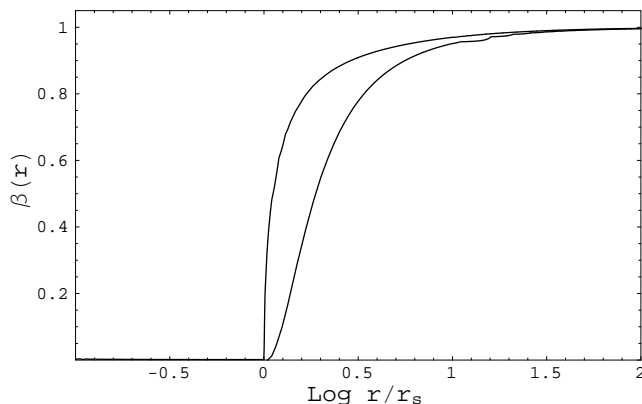


FIG. 10.—Plot of the anisotropy parameter, $\beta(r) \equiv 1 - \overline{v_r^2}/(2\overline{v_t^2})$, for both models. The core is nearly isotropic and becomes nearly radially anisotropic at $10r_s$. The r_c model (upper curve) is slightly more anisotropic than the J_m model (lower curve).

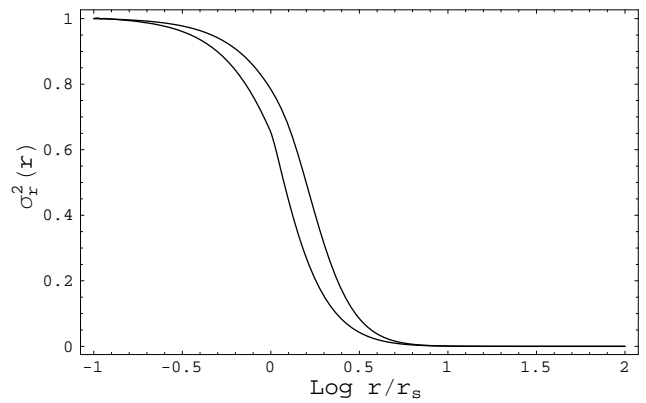


FIG. 11.—Plot of the normalized radial velocity dispersion, $\sigma_r^2(r) = \overline{v_r^2(r)}/\overline{v_r^2(0)}$, for both models. The r_c model (lower curve) is slightly more radially anisotropic than the J_m model (upper curve).

radii ($0.1r_e - 2r_e$) over which the $r^{1/4}$ law provides excellent fits to the brightness profiles of ellipticals (Burkert 1993). The slope in the figure is close to -8 (the standard slope is -7.67), where Σ was normalized to its value at the center unlike the usual normalization by the extrapolated peak value.

The anisotropy profile.—The DF, equation (3), naturally gives radially anisotropic models where most of the mass is outside the core radius. The anisotropy profile and velocity dispersions of the $\mathcal{E}^{3/2}$ models are very similar to that of the T_r models. Figure 10 shows a plot of the run of the anisotropy parameter, β , with radius. Both the r_c and J_m models are very nearly isotropic within the core and rapidly become anisotropic. Figure 11 shows the radial velocity dispersions which indicate that the r_c model is slightly more anisotropic than the J_m model. The dispersion and anisotropy profiles are very similar to Figure 8 of van Albada (1982).

7. DISCUSSION

In § 1 we made an assumption, based on a plausible picture of diffusion in action space, that $A(E) = \text{constant}$; as discussed in § 6, the agreement with simulations is encouraging. However, the physical picture of mixing without friction leads to a constant A only if the constraints are hard and the mixing lasts enough time, two things we cannot lay down a priori. So the success of the simplest such model does teach us that this picture is a good first approximation, possibly improvable.

We now compare and contrast our approach with two earlier papers which can be regarded as fitting into the same broad framework of constrained violent relaxation. MTJ explored DFs with Gaussian and Lorentzian cutoffs in J , multiplied by an exponential function of E ; thus their models have one more parameter, a temperature $1/\beta$ (cf. Stiavelli & Bertin 1987). The infinite temperature limits of their models, in common with our sharply cutoff J_m model, have an asymptotically flat $N(E)$ near $E = 0$. In order to obtain an increasing $N(E)$ with the MTJ models, one requires a negative β . As discussed earlier, our r_c model gives an increasing $N(E)$ without the need for an exponential factor. We therefore find that the r_c model is preferable to the J_m model. We note that even if the cutoff function

$\mathcal{C}(\eta)$ is not as abrupt as given in equation (6), $N(E)$ is expected to behave in a similar fashion.

SH proposed a kinetic model of the wave-particle interaction process, with an associated variational principle analogous to Boltzmann's H -theorem, and made a comparison with their own extensive simulations. Their description of energy changes occurring by a sequence of kicks is in fact close to the picture here. We used this to motivate a *constant* phase space density modulated by a pericenter or angular momentum cutoff and Tremaine's incompleteness factor (T_e/T_r). In contrast, SH assume that the kinetics drives the system to the maximum of its entropy functional. However, their Boltzmann-like factor contains a *negative* temperature (as in the MTJ models), but this equilibrium is meaningful only in systems for which the density of accessible states decreases rapidly with energy (cf. § 73 of Landau & Lifshitz 1980). We suggest that the SH kinetic picture, with which we are in broad agreement, would not actually lead to a negative temperature distribution. The more appropriate physical picture is one of mixing in phase space.

8. CONCLUSIONS AND CAVEATS

We have presented a semianalytic model of violent relaxation that includes a new picture of diffusion in phase space with a novel implementation of the pericenter constraint

and the $1/T_r$ incompleteness factor. Notions of even a partial thermal equilibrium with Boltzmann-like exponential factors play no role—a property we regard as a virtue in describing a collisionless system. The rise in the energy distribution function which such factors (with negative temperatures!) mimicked in earlier work now arises naturally from the pericenter cutoff in our calculation. The resulting properties of density, surface brightness, energy distribution, and anisotropy profiles are in good agreement with simulations. The fact that the properties of the models are parameter free (M and r_s are merely used to normalize) may be considered a virtue, as they demonstrate that the constraints explored here seem to capture the essential details in the case of cold nonrotating collapse. More realistic systems can be obtained if one deviated from the simplifying assumptions and comprehensively explored associated models such as $1/(T_r + T_0)$ in § 5, albeit with more parameters. Even though sophisticated numerical codes now exist to perform N -body experiments, semianalytic models help in understanding their output. They also have the advantage of fitting simulations and observed galaxies reasonably well. Possible directions of future work include a more detailed comparison of our models with numerical simulations, investigations of stability, and extension to axisymmetric systems.

APPENDIX A

THE $\mathcal{E}^{3/2}$ MODEL WITH PERICENTER CUTOFF

We have carried out a detailed study of models with f_0 , the first factor in equation (3), chosen to be $\mathcal{E}^{3/2}$, with both kinds of cutoff, viz., pericenter and angular momentum. Existing work by MTJ uses a Gaussian rather than sharp cutoff in angular momentum. The pericenter cutoff has not been implemented previously, and § 3 gives some details to enable the interested reader to see how the sharply cutoff models are constructed, and other details of its properties along with comparisons to simulations can be found elsewhere (Mangalam & Sellwood 1999). As a first approximation and the simplest model, we consider the distribution function $f_0 = \mathcal{E}^{3/2}$, with a sharp pericenter cutoff at r_c . Then the integral in § 3.1 can be written as

$$\begin{aligned} \mathcal{F}_0(r; \mathcal{E}^{3/2}) &= \frac{1}{\sqrt{2}r^2} \int_0^{J_c^2} dJ^2 \int_0^{B(r, J^2)} d\mathcal{E} \mathcal{E}^{3/2} (-\mathcal{E} + B)^{-1/2} \\ &= \frac{\pi}{\sqrt{8}} (-\Phi)^3. \end{aligned} \tag{A1}$$

Similarly, the integral

$$\mathcal{F}_-(r; \mathcal{E}^{3/2}) = \frac{\pi}{\sqrt{8}} \mathcal{E}_*^3, \tag{A2}$$

but where J_*^2 is the lower limit to J^2 and

$$\mathcal{K}_-(r; \mathcal{E}^{3/2}) = \frac{\pi}{\sqrt{8}} \left(-\Phi - \frac{J_m^2}{2r^2} \right)^3, \tag{A3}$$

where J_m^2 is the lower limit to J^2 . Now the “+” integral works out to be

$$\begin{aligned} \mathcal{F}_+(r; \mathcal{E}^{3/2}) &= \frac{1}{r^2} \int_0^{\mathcal{E}_*} d\mathcal{E} \mathcal{E}^{3/2} [\sqrt{(-\Phi - \mathcal{E})2r^2 - J^2}]_{J_*^2}^{(\mathcal{E} + \Phi_c)r_c^2} \\ &= \frac{\pi}{\sqrt{8}} \mathcal{E}_*^3 \left(1 - \sqrt{\frac{r^2 - r_c^2}{r^2}} \right). \end{aligned} \tag{A4}$$

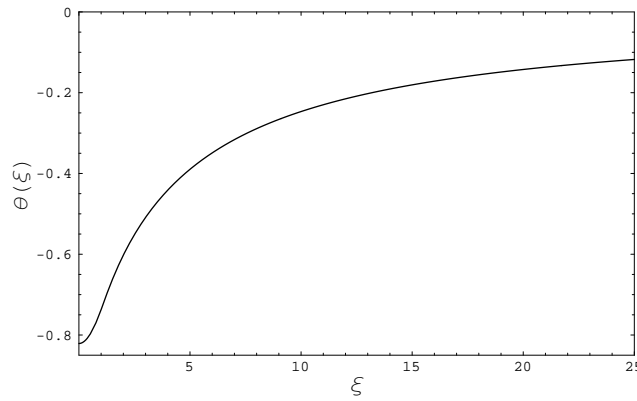


FIG. 12.—Solution for the potential in the $\mathcal{E}^{3/2} - r_c$ model is shown in the figure in units of $0.265 GM/r_c$, where r_c is the unit of radius

Gathering all the integrals in \mathcal{I} , defined above and equation (12), and absorbing the numerical factor into a *positive* constant K , Poisson's equation can be written as

$$\frac{1}{r^2} \frac{d}{dr} (\Phi r^2) = K \begin{cases} -\Phi^3, & r \leq r_c \\ [(r^2 - r_c^2)^{-5/2}/r](\Phi r^2 - \Phi_c r_c^2)^3 - \Phi^3, & r > r_c. \end{cases} \quad (\text{A5})$$

This model is a polytrope of index 3 for $r < r_c$, and we recover the standard results for a distribution function of the form $\mathcal{E}^{3/2}$ without the pericenter cutoff (see Binney & Tremaine 1987, eq. [4-108c]). For $r > r_c$, the contribution to the density is dominated more by orbits with largely radial velocities and the first of the terms limits the orbits to those which have angular momenta less than the bound specified by \mathcal{A}_2 . In the limit of $r_c = 0$, the right-hand side of equation (A5) for $r > r_c$ vanishes as expected. We now scale the radius by $\lambda = r/\xi$ and the potential by $\alpha = \Phi/\theta$, similar to scalings employed for the polytrope problem (with the difference that we have the normalization constant K) and obtain the following relations

$$K\alpha^2\lambda^2 = 1, \quad (\text{A6})$$

$$GM/(\lambda\alpha) = a \equiv - \int_0^{\xi_c} \xi^2 \theta^3 d\xi - \int_{\xi_c}^{\infty} \xi [-(\xi^2 - \xi_c^2)^{-5/2} (\theta \xi^2 - \theta_c \xi_c^2)^3 + \xi \theta^3] d\xi, \quad (\text{A7})$$

where a is a geometric factor that depends on the solution. Here we pick $\lambda/r_c = \xi_c = 1$ [so that $\alpha = GM/ar_c$ and $K = (a/GM)^2$] such that the cutoff radius in these units is unity and it simplifies the task of finding the solution. This model has two parameters, the total mass M and the cutoff radius r_c , and a unique solution can be found from the resulting equation, where $\theta_c = \theta(1) \equiv \theta_1$

$$\frac{1}{\xi^2} \frac{d}{d\xi} (\theta' \xi^2) = \begin{cases} -\theta^3, & \xi \leq 1 \\ \{ [(\xi^2 - 1)^{-5/2}]/\xi \} (\theta \xi^2 - \theta_1)^3 - \theta^3, & \xi > 1, \end{cases} \quad (\text{A8})$$

with the boundary conditions

$$\theta'(0) = 0, \quad \theta(\infty) = 0. \quad (\text{A9})$$

The former is a consequence of an implicit assumption of a nonexistence of a central point mass, and the latter boundary condition is enforced to be consistent with the distribution $f_0 = \mathcal{E}^{3/2} \sim 1/T_r$ vanishing at $\mathcal{E} = 0$. It is interesting to study the asymptotics of this model by changing to a convenient variable $u = 1/\xi$. For $u < 1$, we obtain

$$u^4 \theta''(u) = (\theta - \theta_1 u^2)^3 (1 - u^2)^{-5/2} - \theta^3. \quad (\text{A10})$$

As $r \rightarrow \infty$ or near $u = 0$, we can expand in powers of u to obtain

$$u^4 \bar{\theta}''(u)/\theta_1^2 = -3u^2 \bar{\theta}^2 + 3\bar{\theta}u^4 + (5/2)\bar{\theta}^3 u^2 - u^6 + O(u^7), \quad (\text{A11})$$

where $\bar{\theta} = \theta/\theta_1$, which leads to the following solution of $\theta(u)$ near $u = 0$:

$$\bar{\theta}(u) = c_1 u - (3/2)c_1^2 \theta_1^2 u^2 + O(u^3), \quad (\text{A12})$$

where $c_1 = a/\theta_1$ since $\Phi \rightarrow -GM/r_c u$ or $\theta \rightarrow -au$. As a result the density, ρ , in units of M/r_c^3 asymptotically behaves as

$$\rho = u^4 \theta''(u) = \theta_1^3 \{ -3c_1^2 u^4 + [3c_1 - 9c_1^2 \theta_1^2 + (5/2)c_1^3] u^5 \} + O(u^6). \quad (\text{A13})$$

Hence, as $r \rightarrow \infty$, $\rho \propto r^{-4}$. Now the radius beyond which the leading term dominates, which we call the break radius, is defined as

$$r_b \simeq r_c \left| \frac{1}{c_1} + \frac{5}{6} c_1 - 3\theta_1^2 \right|. \quad (\text{A14})$$

Next we solve equations (A8) and (A9). It is convenient to use Lane-Emden solutions in the region ($0 \leq \xi \leq 1$) and use equation (A10) in the region $1 > u \geq 0$, with the boundary condition $\theta(u=0) = 0$. A sufficiently accurate solution for the region $0 \leq \xi \leq 1$ can be obtained by power series expansions. The solution up to order 12 given in terms of the well depth $\theta(0) = \theta_0$ can be obtained from power series expansions. Using that solution for a trial well depth, θ_0 , $\theta(u=1)$, and $\theta'(u=1) = -\theta'(\xi=1)$ are calculated and equation (A10) is numerically integrated to $\theta(u=0)$. A value of θ_0 , for which the boundary condition $\theta(u=0) = 0$ is satisfied, is determined iteratively. This occurs for

$$\theta_0 = -0.821, \quad \theta'(u=1) = -0.15264, \quad \theta(u=1) = -0.737234 \quad (\text{A15})$$

and the corresponding $\theta(\xi)$ is shown in Figure 12. Note that for this solution, $a = 3.38$.

REFERENCES

- Binney, J., & Tremaine, S. 1987, *Galactic Dynamics* (Princeton: Princeton Univ. Press)
- Burkert, A. 1993, *A&A*, 278, 23
- Dejonghe, H. 1987, *ApJ*, 320, 477
- Jaffe, W. 1987, in *Structure and Dynamics of Elliptical Galaxies*, ed. T. De Zeeuw (Dordrecht: Reidel), 511
- Landau, L. D. 1937, *Zh. Eksp. Teor. Fiz.*, 7, 203
- Landau, L. D., & Lifshitz, E. M. 1980, *Statistical Physics* (Oxford: Pergamon)
- Lichtenberg, A. J., & Lieberman, M. A. 1983, *Regular and Stochastic Motion* (New York: Springer)
- Lifshitz, E. M., & Pitaevskii, L. P. 1981, *Physical Kinetics* (Oxford: Pergamon)
- Lynden-Bell, D. 1967, *MNRAS*, 136, 101
- Mangalam, A., & Sellwood, J. A. 1999, in preparation
- Merrit, D., Tremaine, S., & Johnstone, D. 1989, *MNRAS*, 236, 829 (MTJ)
- Moore, B., Governato, F., Quinn, T., Stadel, J., & Lake, G. 1998, *ApJ*, 499, L5
- Spergel, D. N., & Hernquist, L. 1992, *ApJ*, 397, L75 (SH)
- Sridhar, S. 1987, *J. Astrophys. Astron.*, 8, 257
- Stiavelli, M., & Bertin, G. 1987, *MNRAS*, 229, 61
- Tormen, G., Bouchet, F. R., & White, S. D. M. 1997, *MNRAS*, 286, 865
- Tremaine, S. 1987, in *Structure and Dynamics of Elliptical Galaxies*, ed. T. De Zeeuw (Dordrecht: Reidel), 367
- Tremaine, S., Henon, M., & Lynden-Bell, D. 1986, *MNRAS*, 219, 285
- van Albada, T. S. 1982, *MNRAS*, 201, 939
- Yankov, V. V. 1994, *JETP*, 60(3), L171